Article ID: 1006-8775(2020) 04-0483-12

Study on the Structure of a Horizontal Shear Line over the Tibetan Plateau Based on CRA−Interim Datasets and Its Comparison with ERA−Interim Datasets

YAO Xiu-ping (姚秀萍)[1], ZHANG Shuo (张 硕)[2], BAO Xiao-hong (包晓红)[1, 3],
SHI Chun-xiang (师春香)[4], LIU Jing-wei (刘景卫)[4]
(1. China Meteorological Administration Training Centre, Beijing 100081 China; 2. Beijing Institute of Applied Meteorology, Beijing 100029 China; 3. Chinese Academy of Meteorological Sciences, Beijing 100081 China; 4. National Meteorological Centre, Beijing 100081 China)

Abstract: The CRA-Interim trial production of the global atmospheric reanalysis for 10 years from 2007 to 2016 was carried out by the China Meteorological Administration in 2017. The structural characteristics of the horizontal shear line over the Tibetan Plateau (TPHSL) based on the CRA-Interim datasets are examined by objectively identifying the shear line, and are compared with the analysis results of the European Centre for Medium-Range Weather Forecasts reanalysis data (ERA-Interim). The case occurred at 18UTC on July 5, 2016. The results show that both of the ERA-Interim and CRA-Interim datasets can well reveal the circulation background and the dynamic and thermal structure characteristics of TPHSL, and they have shown some similar features. The middle and high latitudes at 500 hPa are characterized by the circulation situation of "two troughs and two ridges", and at 200 hPa, the TPHSL is located in the northeast quadrant of the South Asian High Pressure (SAHP). The TPHSL locates in the positive vorticity zone and passes through the positive vorticity center corresponding to the ascending motion. Near the TPHSL, the contours of pseudo-equivalent potential temperature (θ_{se}) tend to be intensive, with a high-value center on the south side of the TPHSL. The TPHSL can extend to 460 hPa and vertically inclines northward. There is a positive vorticity zone near the TPHSL which is also characterized by the northward inclination with the height, the ascending motion near the TPHSL can extend to 300 hPa, and the atmospheric layer above the TPHSL is stable. However, the intensities of the TPHSL's structure characteristics analyzed with the two datasets are different, revealing the relatively strong intensity of geopotential height field, vertical velocity field, vorticity field and divergence field from the CRA-Interim datasets. In addition, the vertical profiles of the dynamic and water vapor thermal physical quantities of the two datasets are also consistent in the east and west part of the TPHSL. In summary, the reliable and usable CRA-Interim datasets show excellent properties in the analysis on the structural characteristics of a horizontal shear line over the Tibetan Plateau.

Key words: CRA-Interim datasets; ERA-Interim datasets; horizontal shear line over the Tibetan Plateau; structure
CLC number: P462.62 **Document code:** A
https://doi.org/10.46267/j.1006-8775.2020.042

1 INTRODUCTION

Atmospheric reanalysis data integrates data assimilation, numerical model, and data processing technology, so it reflects the comprehensive meteorological strength of a country. Since the launch of the first Global Atmospheric Research Programme (FGGE) in 1979, the scientific and operational value of the atmospheric reanalysis field has been acknowledged. The global reanalysis products are developed into the third generation in 2011; among them, the ERA-Interim datasets are the third-generation reanalysis products with higher spatial resolution and longer time series on the basis of the second-generation reanalysis product (ERA-40), provided by the European Centre for Medium-Range Weather Forecasts (ECMWF) (Berrisford et al.[1]). There are significant differences among different reanalysis datasets due to the difference of assimilation schemes, applied data and deviation correction methods (Tian et al.[2]). It is found that the ground temperature data of ERA-interim performs best in the Tibetan Plateau (TP) by comparing the applicability of geothermal data from ERA-interim, NCEP1 and NCEP2 reanalysis datasets (He et al.[3]). The results show that the geopotential height field data from the ERA-interim reanalysis datasets has the best correlation with the sounding data in the TP by comparing with the NCEP1 and other 7 reanalysis datasets. The ERA-Interim reanalysis datasets can better reflect the variation of geopotential height in the TP area (Hu et al.[4]). The thermal conditions described by the ERA-interim, ERA-40 and JRA-25 reanalysis datasets are more accurate according to a comparative study of six different reanalysis datasets in the TP (Liu et al.[5]).

Received 2020-04-26 **Revised** 2020-08-15 **Accepted** 2020-11-15
Funding: National Science Foundation of China (42030611, 91937301); The Second Tibetan Plateau Scientific Expedition and Research (STEP) Program (2019QZKK0105)
Biography: YAO Xiu-ping, Professor, Ph. D., primarily researching and teaching on synoptic dynamics.
Corresponding author: YAO Xiu-ping, e-mail: yaoxp@cma.gov.cn

The first generation of 40-year global atmospheric reanalysis datasets (CRA-40) was launched by the China Meteorological Administration (CMA) in 2013. In addition to importing satellite data from the third generation of international reanalysis products, CRA-40 has also collected the latest satellite products released in recent years (Wang et al. [6]). This dataset is the first set of global atmospheric reanalysis products owned by China, which is based on the collective-variational hybrid assimilation technology and integrates the conventional observational data, sounding and ground data of Fengyun satellites. This product focuses on serving major national strategies, facilitating meteorological disaster prevention and mitigation, practicing the concept of "global monitoring, global forecasting and global service". And it will support global monitoring, provide inspection for global forecasting, guarantee for global services, operational guidance and data services for member countries of the World Meteorological Organization (WMO), as well as the countries along the "Belt and Road Initiative" route and the Silk Road economic core area. The pre-assessment of the 10-year (2007–2016) global atmospheric CRA-Interim Reanalysis trial product was completed by CMA in 2017. The results show that the root mean square error of global wind field is superior to that of the CFSR (Climate Forecast System Reanalysis), which is equivalent to the error of JRA-55 (Japanese 55-year Reanalysis) product, and its performance has reached the level of international third-generation reanalysis product. Since June of 2018, the CRA-interim which is the 10-year product from CRA-40 has been widely used for research and applications after detailed assessment and operational review.

TP is known as the third pole of the Earth, whose dynamic and thermal effects have an important impact on the energy and water cycles in East Asia and the world. It also affects the local weather and climate in the plateau, the atmospheric environment in East Asia and its surrounding areas and even changes in the global atmospheric circulation (Flohn [7]; Yin [8]; Tanaka et al. [9]; Ueda [10]; Yao et al. [11]; Zhao et al. [12]; Murakami [13]). However, due to the small number of observation stations and limited measured data, the study of plateau weather relies on reanalysis data which has better spatial continuity and longer time series.

Since the 1950s, various studies on the TP not only have deepened the understanding of the atmospheric movement characteristics over the plateau, but also have found that a unique low-geopotential-height system on the plateau—the plateau shear line, is generated under the dynamic and thermal forces of the plateau's special terrain (Luo [14]; Xu [15]; Shen et al. [16]; Gao and Yao [17]). The results show that the precipitation in the plateau and other areas is caused by the plateau shear (Zhang et al. [18]). The severe weather such as rainstorm, thunderstorm and blizzard in the surrounding areas of the plateau, and even the precipitation processes eastern China are caused by the eastward movement of the plateau shear line (Ye et al. [19]; Qiao and Tan [20]). The plateau shear line is one of the triggers for the occurrence of severe weather in the plateau and surrounding areas (Li [21]; Li et al. [22]; Yu et al. [23]; Yao et al. [24]).

Previous studies on the plateau shear line mainly adopted observational data. Based on the analysis of the 1979 Qinghai-Tibet Plateau atmospheric science experimental observational data, it is found that the plateau shear line is a shallow weather system, which locates within the cyclonic circulation along the horizontal direction, with the strong east-west airflow. Meanwhile, a basic understanding of the occurrence frequency, moving position and forming conditions of the shear line is also revealed (see Qinghai-Tibet Plateau Meteorological Research Lhasa Battle Group [25]; Tao et al. [26]). In recent years, the application of reanalysis data has become the basic way for plateau research (Tao et al. [27]; Min et al. [28]; Li et al. [22]). According to the evaluation of different reanalysis datasets' applicability on the plateau (Liu et al. [5]), the reanalysis data provided by the European Centre for Medium-Range Weather Forecasts (referred to as ERA-Interim; Dee et al. [29]) are mostly used. Zhang et al. [18] used ERA-Interim reanalysis datasets to analyze the plateau shear line and found that more than 60% of the rainstorms in the plateau during the rainy season from June to August are related to the plateau shear line. In the researches of TP, the ERA-Interim reanalysis data has a good performance in the study of plateau low-geopotential-height systems (Liu and Li [30]; Zhang et al. [18]; Guan et al. [31]).

This paper proposes to reveal the structure characteristics of the shear line based on the 10-year CRA-Interim datasets and compare it with the ERA-Interim datasets, in order to evaluate the performance and feasibility of the CRA-Interim datasets in the study of a horizontal shear line over the Tibetan Plateau.

2 DATA AND METHODOLOGY

2.1 *Data*

Two kinds of datasets are used in this paper. One is the China Meteorological Administration's Global Atmospheric Reanalysis Intermediate Product (CRA-Interim) with a time resolution of 4 times daily and a spatial resolution of $0.3125° \times 0.3125°$, which includes 126 variables with 47 levels in the vertical direction. The other is the European Centre for Medium-Range Weather Forecasts (ECMWF) ERA-Interim reanalysis data with a time resolution of 4 times daily, a spatial resolution of $0.25° \times 0.25°$ and 27 levels in the vertical direction.

2.2 *Objective identification of the TPHSL*

The identification of the TPHSL is based on the objective identification technology proposed by Ma et al. [32], and the objective method proposed by Zhang et al. [18] is used to determine the plateau shear line.

$$\begin{cases} \partial u/\partial y < 0 \\ \zeta > 0 \\ u = 0 \end{cases},$$

where u represents the zonal wind speed, ζ represents the relative vorticity, x is the meridional coordinate and y is the zonal coordinate.

The case of TPHSL at 18UTC on July 5, 2016 is selected as the research object in this paper.

As shown in Fig. 1a, the TPHSL analyzed with the CRA-Interim datasets is discontinuous and is roughly broken into three sections, which are located at (80°–85°E, 35°N), (90°–95°E, 35°N) and (97°–103°E, 35° N), respectively. The shear line locates in the cyclonic circulation, with the large wind speed at (90°–95°E, 35°N) around the TPHSL. The southerly airflow is significant on the south side of the TPHSL, and the north side of the TPHSL is dominated by the easterly airflow. The TPHSL analyzed with the ERA-Interim datasets roughly spans the main body of the plateau (80°–97°E, 34°–35°N) with an obvious cyclonic circulation nearby. The southerly airflow at (90°–95° E, 35° N) near the TPHSL is more conspicuous compared with that from the CRA-Interim datasets.

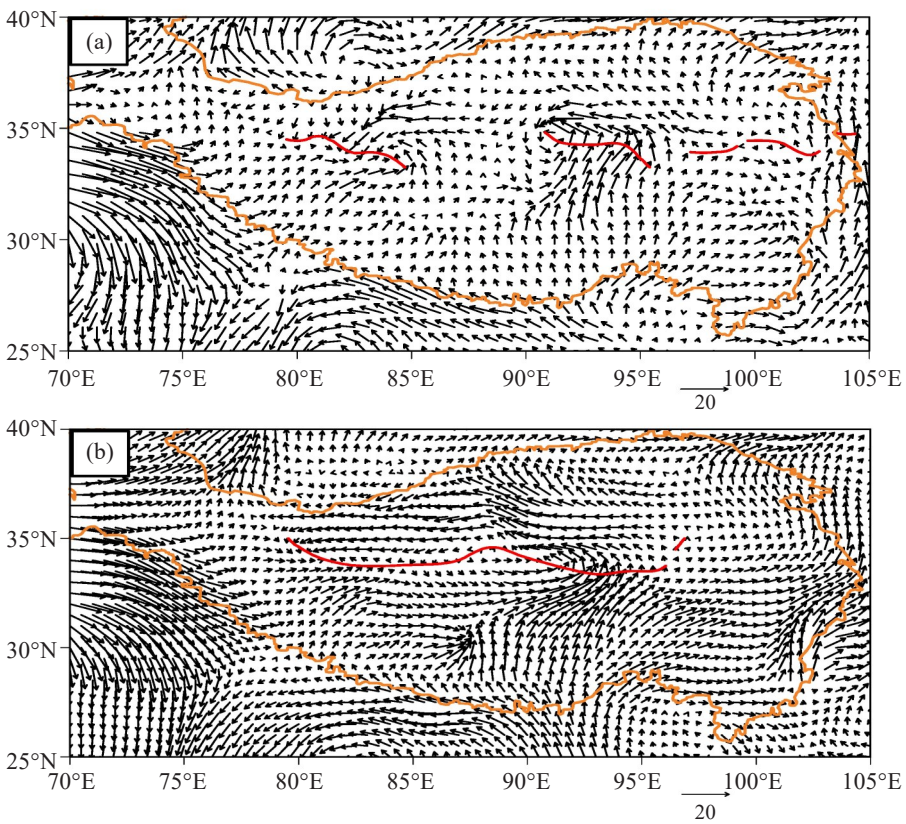

Figure 1. Wind fields at 500 hPa at 18UTC on July 5, 2016 from the (a) CRA-Interim datasets and (b) ERA-Interim datasets. The thick red solid line represents TPHSL; the orange boundary line represents the plateau boundary over 3000m above sea level, and the same in the following figure.

3 COMPARATIVE ANALYSIS OF THE CIRCULATION BACKGROUND

3.1 *Circulation field at 500 hPa*

The circulation situation at 500 hPa can be seen from Fig. 2, and the basic characteristics analyzed with the two datasets are consistent. The circulation situation in the middle and high latitudes at 500 hPa is "two troughs and two ridges", and the TPHSL is located in the front area of the middle and high-latitude trough and the rear area of the ridge, i.e. (80°–103°E, 33°–35°N). In addition, there is a low-pressure center at (81°E, 21°N) on the south side of the TPHSL. Overall, the intensity of 500 hPa geopotential height field analyzed with the CRA-Interim datasets is stronger than that from the ERA-Interim datasets.

3.2 *Circulation field at 200 hPa*

The ridge line of the South Asia High Pressure (SAHP) shows an east-west direction, and the TPHSL locates in the lower northeast quadrant of the SAHP (Fig. 3). However, the intensity of SAHP analyzed with the CRA-Interim datasets is obviously stronger than that from the ERA-Interim datasets.

4 COMPARISON AND ANALYSIS OF DYNAMIC STRUCTURE CHARACTERISTICS

4.1 *Horizontal structure characteristics*

In Fig. 4, the TPHSL is located in the positive vorticity zone, and passes through the positive vorticity centers. The characteristics analyzed with the two

datasets are consistent, while the difference is mainly in the intensity of the vorticity zone. There is a maximum vorticity center located at (91°E, 35°N) with an intensity of 20×10^{-5} s^{-1} in the results from the CRA-Interim datasets (Fig. 4a). Whereas for the ERA-Interim datasets, there are two maximum positive vorticity centers located at (82°E, 34°N) and (92°E, 33°N), reaching 10×10^{-5} s^{-1} and 15×10^{-5} s^{-1}, respectively (Fig. 4b).

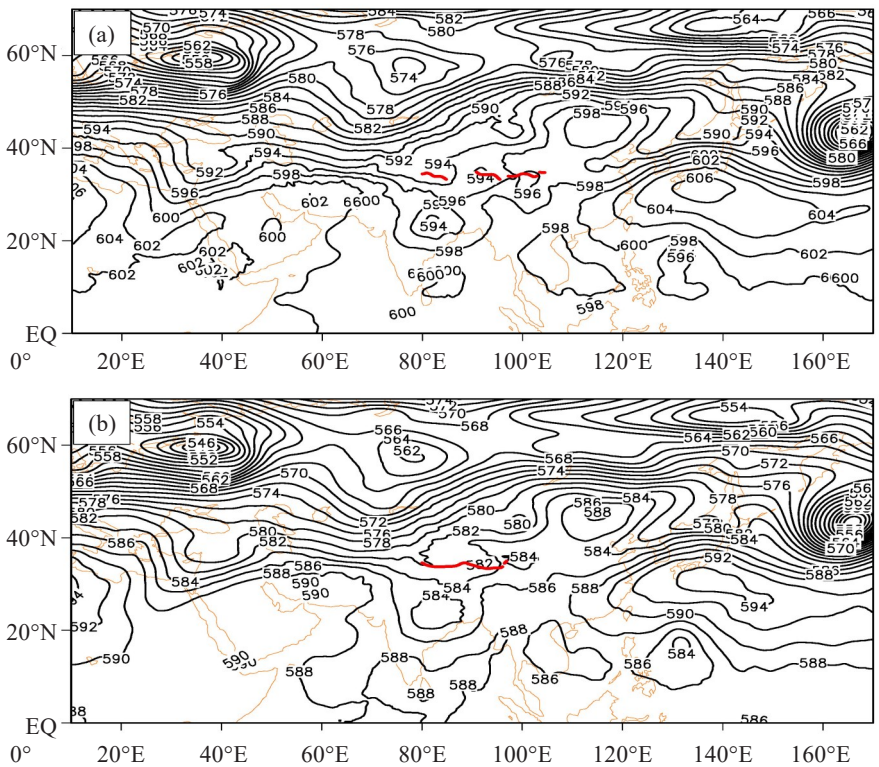

Figure 2. Geopotential height fields at 500 hPa 18UTC on July 5, 2016 analyzed with the (a) CRA-Interim datasets and (b) ERA-Interim datasets. The thick red solid line represents TPHSL, and the black thin solid line represents potential height (units: dagpm). Other parts are the same as those of Fig. 1 and the same in the following figure.

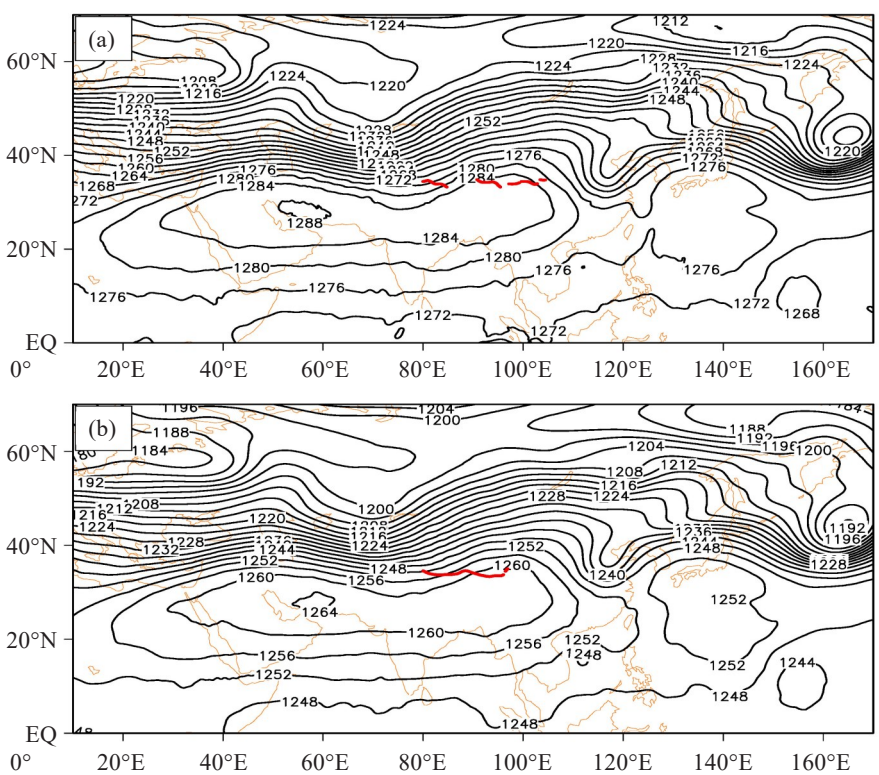

Figure 3. Geopotential height fields at 200 hPa at 18UTC on July 5, 2016 analyzed with the (a) CRA-Interim datasets and (b) ERA-Interim datasets. The thick red solid line represents TPHSL, and the black thin solid line represents potential height (units: dagpm).

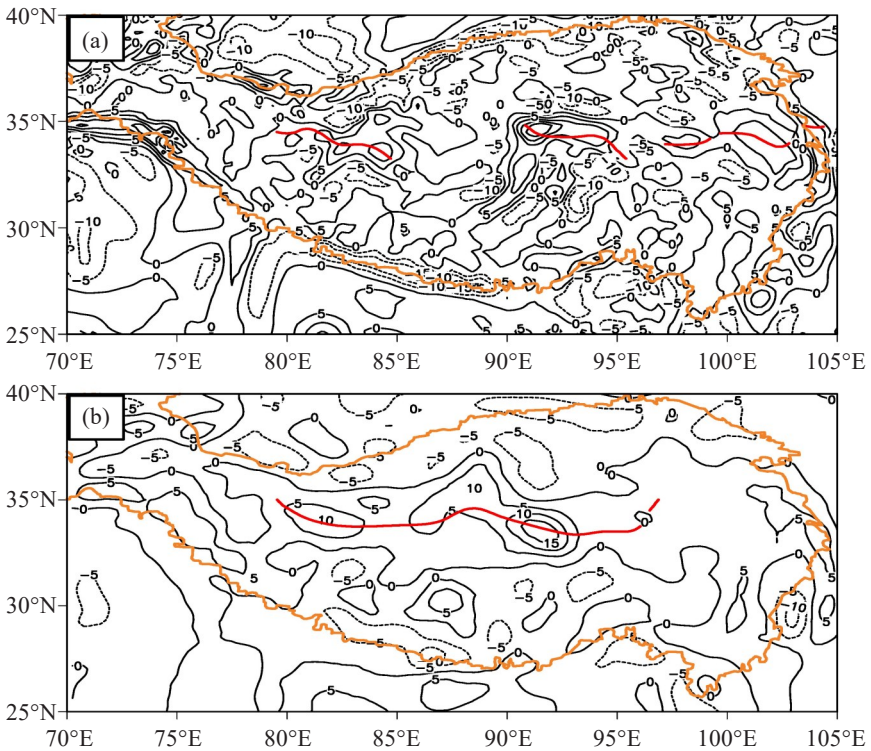

Figure 4. Relative vorticity at 500 hPa at 18UTC on July 5, 2016 analyzed with the (a) CRA-Interim datasets and (b) ERA-Interim datasets. The thick red solid line represents TPHSL, and the black thin solid line represents vorticity (units: 10^{-5} s^{-1}).

The TPHSL is located in the convergence zone at 500 hPa (Fig. 5), and the intensity of the divergence field analyzed with the CRA-Interim datasets is stronger. There are two strong convergence centers on the TPHSL, reaching -20×10^{-5} s^{-1} and -12×10^{-5} s^{-1}, respectively. The area (97°–103°E, 35°N) of the TPHSL is located in the non-divergence zone analyzed with the ERA-Interim datasets (Fig. 5b). There is a strong convergence center at (92°E, 34°N) with a value of -4×10^{-5} s^{-1}.

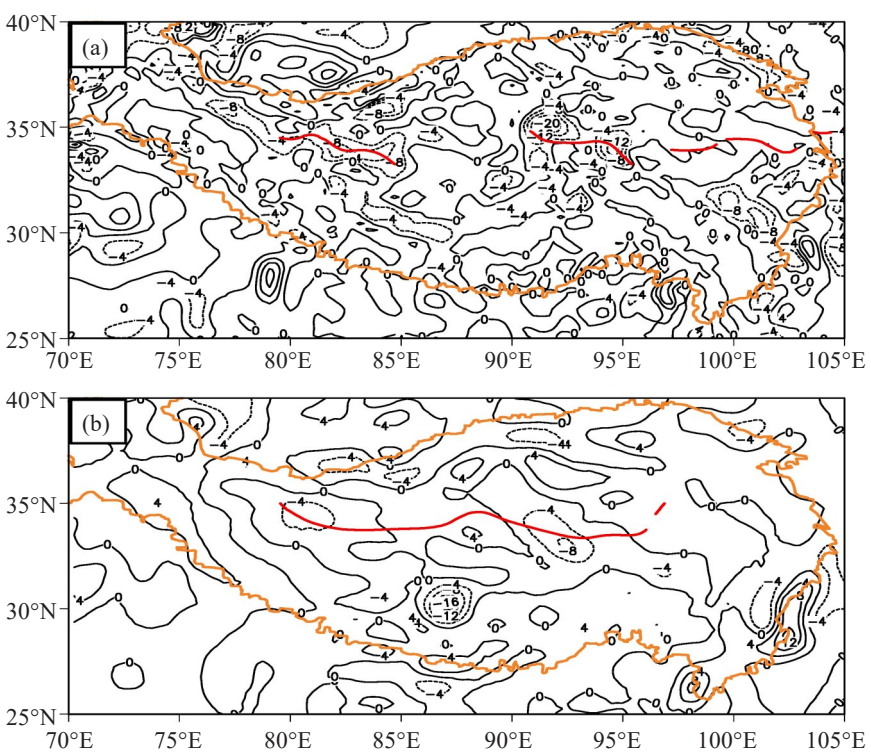

Figure 5. Divergence at 500 hPa at 18UTC on July 5, 2016 analyzed with the (a) CRA-Interim datasets and (b) ERA-Interim datasets. The thick red solid line represents TPHSL, and the black thin solid line represents divergence (units: 10^{-5} s^{-1}).

As can be seen from Fig. 6 that the vertical upward movement is mainly near the TPHSL at 500 hPa, and the rising speed analyzed with the two datasets is equivalent. For CRA-Interim datasets, there is a maximum upward movement center at (90°–95°E, 35°N), with a rising speed of -100×10^{-2}Pa s^{-1} (Fig. 6a). A weak sinking motion and an ascending motion occur in the eastern part (97°–103° E, 35° N) and the western part (80°–85° E, 35° N) of the TPHSL, respectively, with the maximum ascending speed of -50×10^{-2}Pa s^{-1}. For ERA-Interim datasets, there are two upward movement centers located at (82° E, 34° N) and (92° E, 34° N), reaching -20×10^{-2} Pa s^{-1} and -60×10^{-2} Pa s^{-1} (Fig. 6b), respectively.

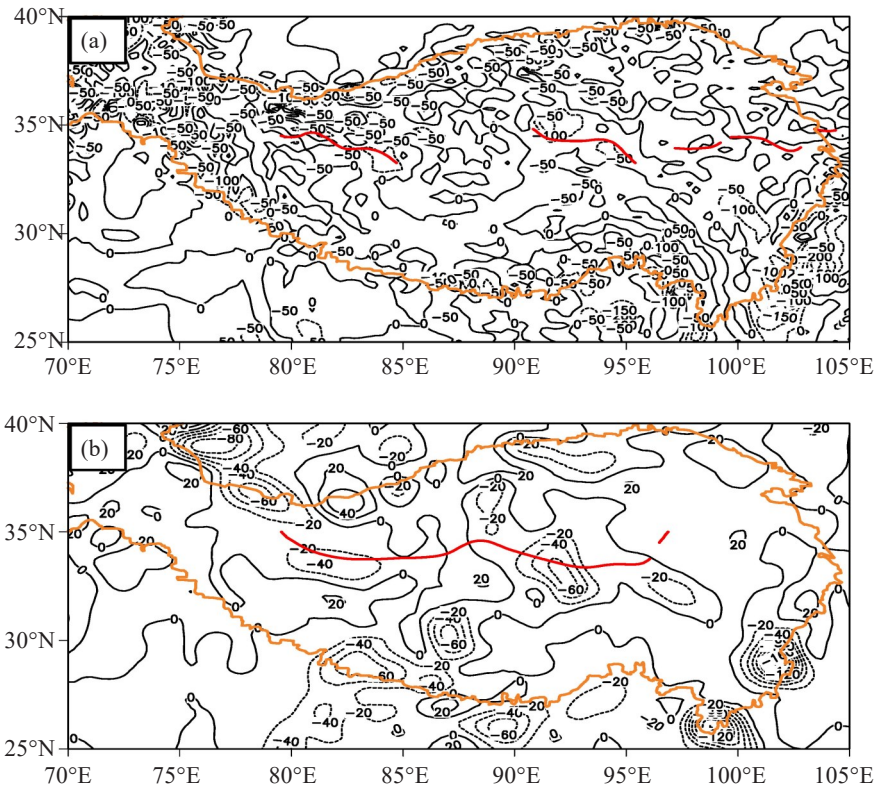

Figure 6. Vertical velocity at 500 hPa at 18UTC on July 5, 2016 analyzed with the (a) CRA-Interim datasets and (b) ERA-Interim datasets. The thick red solid line represents TPHSL, and the black thin solid line represents vertical velocity (units: 10^{-2}Pa s^{-1}).

4.2 *Vertical structural features*

Figure 7 shows the relative vorticity and the vertical velocity along the vertical section of 84° E. The TPHSL inclines northward from the lower layer to the upper layer, which can reach 460 hPa. The TPHSL corresponds well with the positive vorticity belt, which also inclines northward with the height and extends higher than the TPHSL. The maximum intensity in the center of the positive vorticity at 500 hPa analyzed with the CRA-Interim datasets reaches about 12×10^{-5} s^{-1}. While that from the ERA-Interim datasets is only about 4×10^{-5} s^{-1}. According to the vertical velocity along the vertical section of 84° E, the TPHSL corresponds well with the strong upward motion. The rising motion center analyzed with the CRA-Interim datasets is located at about 500 hPa with the maximum value of -80×10^{-2}Pa s^{-1}, while that analyzed with the ERA-Interim datasets only reaches -10×10^{-2}Pa s^{-1}.

To summarize, the characteristics of the relative vorticity analyzed with the two datasets are consistent, but the characteristics of the vertical velocity are different.

Figure 8 shows the divergence and the vertical velocity distributions of the TPHSL in the vertical direction. There is a significant difference in the characteristics of divergence field analyzed with the two datasets. For the CRA-Interim datasets, the divergence belt inclines northward from the lower layer to the upper layer, reaching about 400 hPa, and the TPHSL is completely in the convergence zone, with the maximum value in the convergence center reaching -9×10^{-5} s^{-1} (Fig. 8a). While for the ERA-Interim datasets, the TPHSL is located in the non-divergent zone, and there is a weak convergence zone between 600 and 500 hPa (Fig. 8b).

5 COMPARISON AND ANALYSIS OF THERMAL STRUCTURE CHARACTERISTICS

5.1 *Horizontal thermal structure*

The θ_{se} analyzed with the two datasets is similar in the intensity and consistent in the magnitude (Fig. 9). The TPHSL is located in the area with a large meridional gradient of θ_{se}(Fig. 9a). For the ERA-Interim datasets, this feature is more significant as shown in Fig. 9b, and

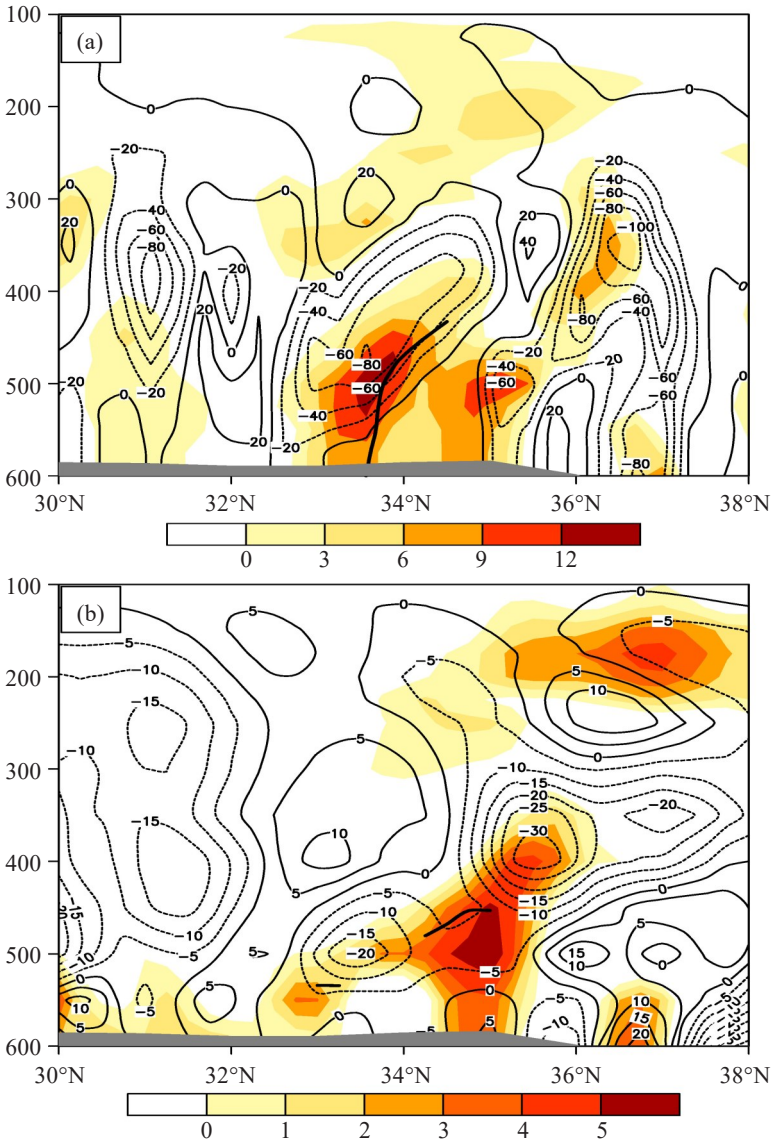

Figure 7. Relative vorticity and vertical velocity along the vertical section of 84°E at 18UTC on July 5, 2016 analyzed with the (a) CRA-Interim datasets and (b) ERA-Interim datasets. The thick black solid line represents TPHSL, the shaded denotes positive vorticity (units: 10^{-5} s^{-1}); the thin black solid line represents vertical velocity (units: 10^{-2}Pa s^{-1}); the gray shadow represents plateau, and the same in the following figure.

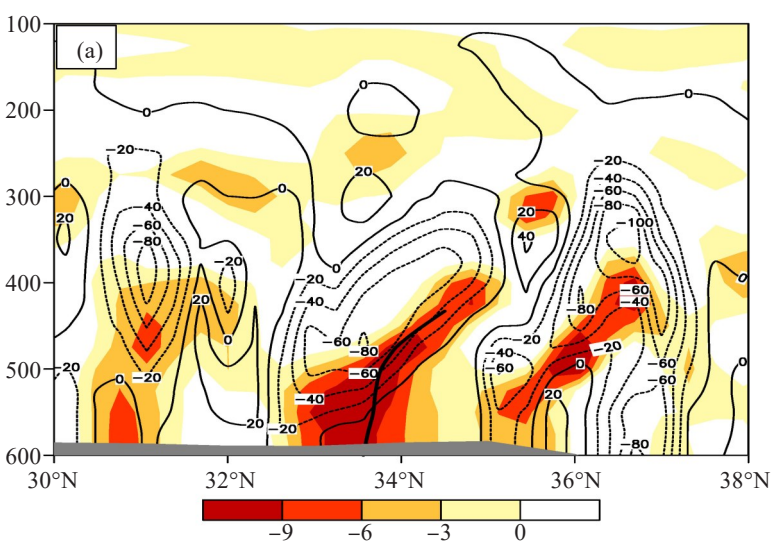

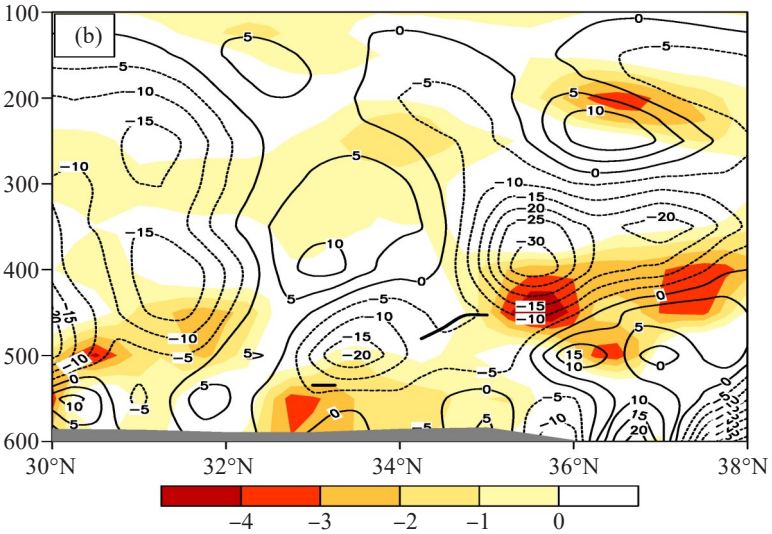

Figure 8. Divergence and vertical velocity along the vertical section of 84°E at 18UTC on July 5, 2016 analyzed with the (a) CRA-Interim datasets, and (b) ERA-Interim datasets. The thick black solid line represents TPHSL, and the shaded denotes negative divergence (units: 10^{-5} s^{-1}); the thin black solid line represents vertical velocity (units: 10^{-2}Pa s^{-1}).

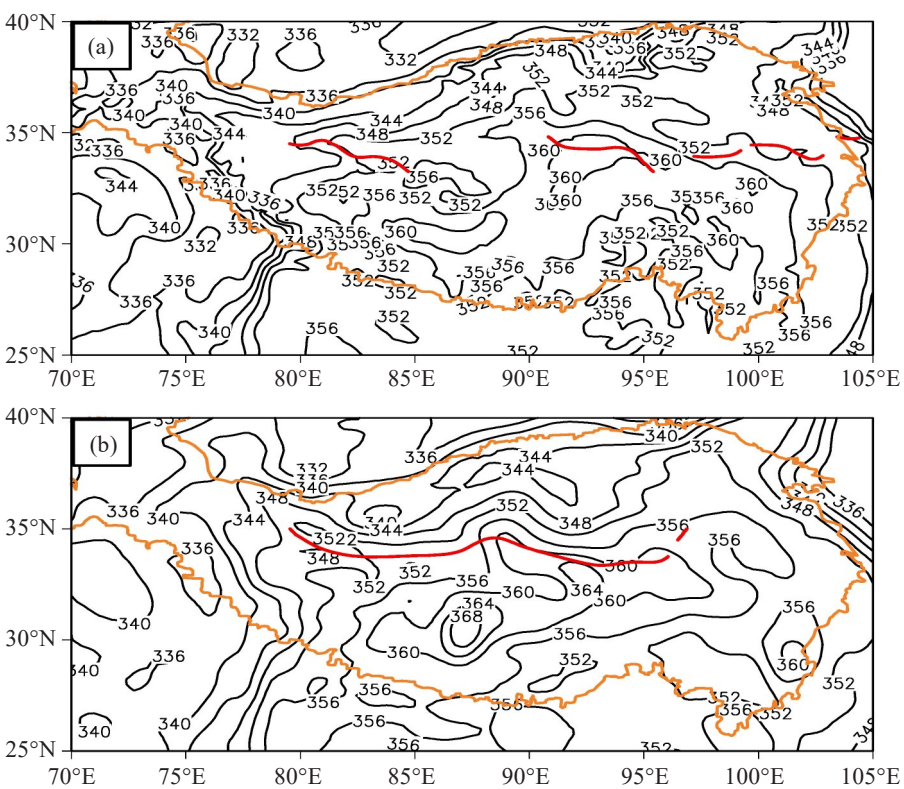

Figure 9. Pseudo-equivalent potential temperature (θ_{se}) at 500 hPa at 18UTC on July 5, 2016 analyzed with the (a) CRA-Interim datasets and (b) ERA-Interim datasets. The thick red solid line represents TPHSL, and the thin black solid line represents θ_{se} (units: K).

there is a high-temperature and high-humidity center at (87°E, 31°N) on the south side of the TPHSL.

5.2 *Vertical thermal structure*

There is a warmer and moister region on the south side of the TPHSL than that on the north (Fig. 10). According to the distribution of θ_{se}, the atmosphere is convectively stable above 300 hPa. The TPHSL is located in the transition zone between the warm-moist zone on the south side and the cold-dry zone on the north side (Fig. 10a). For the ERA-Interim datasets, the TPHSL tilts northward to the north side and locates in the relatively dry and cold area (Fig. 10b). In addition, the contours of θ_{se} near the TPHSL are intensive, which represents the structure of the front area.

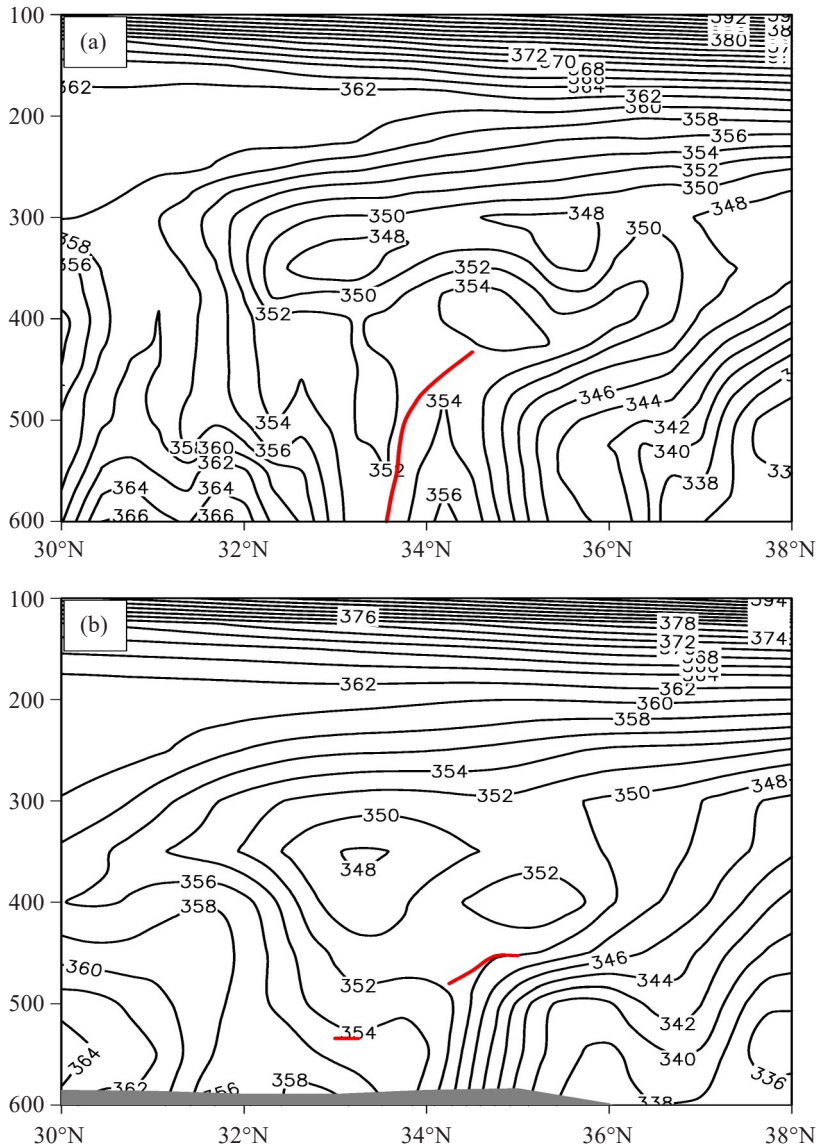

Figure 10. θ_{se} along the vertical section of 84°E at 18UTC on July 5, 2016 analyzed with the (a) CRA-Interim datasets, and (b) ERA-Interim datasets. The thick red solid line represents TPHSL and the thin black solid line represents θ_{se} (units: K).

6 COMPARISON FOR VERTICAL PROFILE OF PHYSICAL QUANTITY

Since the TPHSL analyzed with the CRA-Interim datasets is mainly divided into (80°–85°E, 33°–35°N) (west) and (90°–95°E, 33°–35°N) (east), the vertical profiles of physical quantity are analyzed for the east and west part of the TPHSL.

The distribution of each physical quantity analyzed with the two datasets is basically the same in the vertical direction, and the two parts fit well (Fig. 11). Overall, the vertical velocity distributions analyzed with the two datasets (Fig. 11c1 and 11c2) are quite consistent in the region of (90°–95°E, 33°–35°N), and the magnitude is almost the same. While in the region (80°–85°E, 33°–35°N), the value of vertical velocity analyzed with the CRA-Interim datasets is larger between 500 and 400 hPa near the TPHSL. In addition, according to the vertical profiles of meridional wind (Fig. 11b1 and 11b2), it is different between the east side and the west side between 300 and 150 hPa. The characteristics and magnitude analyzed with the two datasets are relatively consistent in the region of (80°–85°E, 33°–35°N), while there are opposite variations between 300 and 150 hPa in the region of (90°–95°E, 33°–35°N).

Overall, the characteristics and magnitude of the dynamic field analyzed with the two datasets are still similar in the east and west part of the TPHSL, and are more similar in the east part of the TPHSL below 300 hPa.

Figure 12 shows the vertical profiles of temperature, θ_{se} and water vapor flux divergence analyzed with the two datasets. Compared with the dynamic field, the water vapor thermal fields analyzed with the two datasets are more consistent. Among them, the temperature distribution analyzed with the two

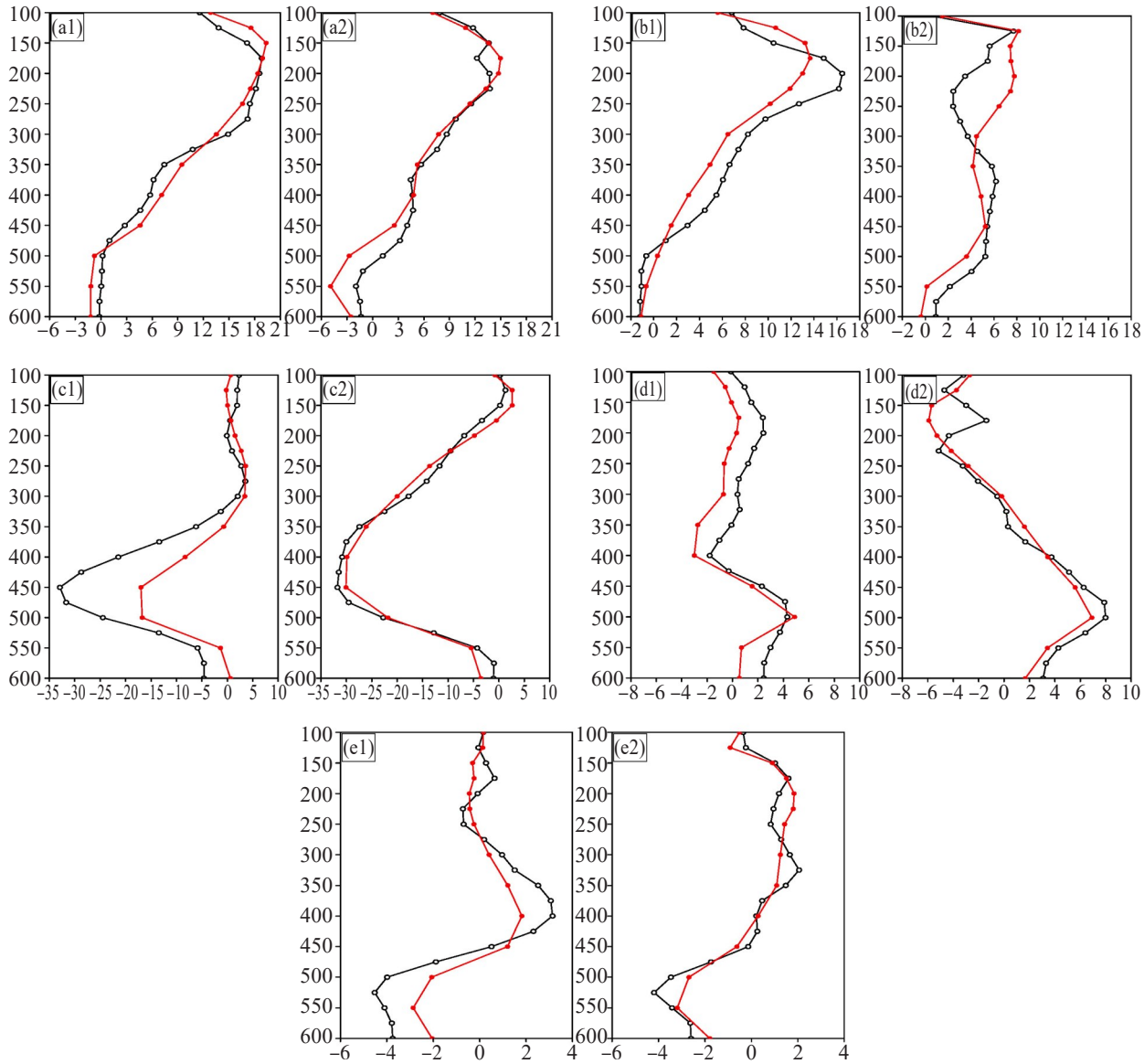

Figure 11. Vertical profiles of average physical quantities near the TPHSL analyzed with the CRA-Interim datasets (black line) and ERA-Interim datasets (red line). a: *U*, units: m s^{-1}; b: *V*, units: m s^{-1}; c: ω, units: 10^{-2}Pa s^{-1}; d: vorticity, units: 10^{-5} s^{-1}; e: divergence, units: 10^{-5} s^{-1}; a1, b1, c1, d1 and e1 for the west part (80°–85°E, 33°–35°N); a2, b2, c2, d2 and e2 for the east part (90°–95°E, 33°–35°N).

datasets is almost the same in the regions of (80°–85°E, 33°–35°N) and (90°–95°E, 33°–35°N), and the profiles almost coincide too (Fig. 12a1 and 12a2). The characteristics of θ_{se} (Fig. 12b1 and 12b2) between the two datasets are also quite consistent. Related research (Liu et al. [29]) have shown that the ERA-Interim reanalysis data is more accurate in reflecting the thermal conditions in the plateau. Therefore, the thermal data of the CRA-Interim datasets is feasible in reflecting the thermodynamic structure of the TPHSL. According to Fig. 12c1, the water vapor flux divergence analyzed with the CRA-Interim datasets is larger. In contrast, the capability of CRA-Interim datasets in the water vapor flux divergence is better in the region of (90° – 95° E, 33°–35°N) (Fig. 12c2).

7 CONCLUSIONS AND DISCUSSION

Based on the CRA-Interim datasets and the ERA-Interim datasets, the structural features of the TPHSL at 18UTC on July 5, 2016 were revealed and compared. The main conclusions are as follows.

(1) The structural features of the TPHSL revealed by the two datasets are quite similar. The TPHSL is in the east-west direction horizontally, and can extend to about 460 hPa with the characteristic of northward inclination. The TPHSL analyzed with the ERA-Interim datasets at 500 hPa is continuous, while it breaks into three segments at 500 hPa for the CRA-Interim datasets.

(2) The characteristics of the geopotential height revealed by the two datasets are basically consistent with each other. The circulation situation of "two troughs and

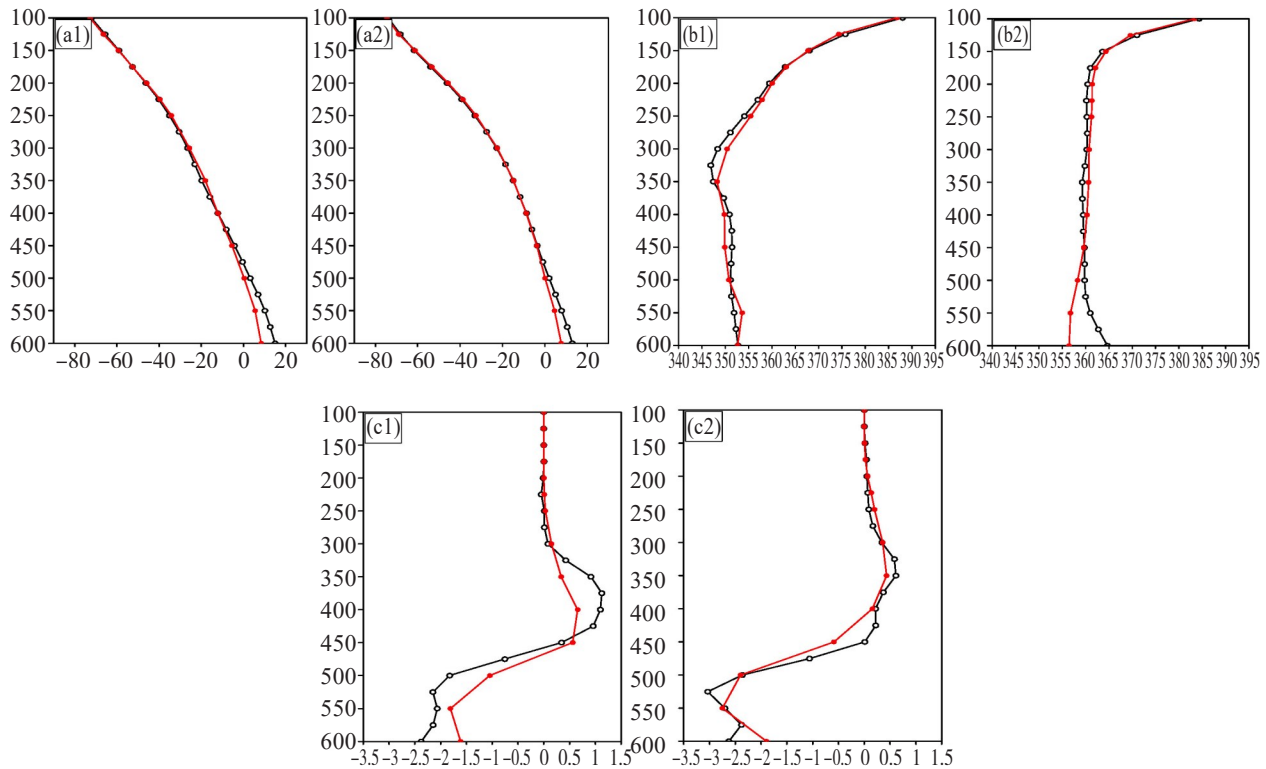

Figure 12. Vertical profiles of average physical quantities near TPHSL analyzed with the CRA-Interim datasets (black line) and ERA-Interim datasets (red line). a: *T*, units: K; b: θ_{se}, units: K; c: water vapor flux divergence, units: 10^{-5}g s^{-1}cm^{-2}hPa^{-1}; a1,b1 and c1 for the west part (80°–85°E, 33°–35°N); a2, b2 and c2 for the east part (90°–95°E, 33°–35°N).

two ridges" is found in the middle and high latitudes at 500 hPa, but the intensity of geopotential height analyzed with the CRA-Interim datasets is slightly stronger. The TPHSL is located in the lower northeast quadrant of the SAHP, and the intensity of the SAHP analyzed with the CRA-Interim datasets is also stronger.

(3) The dynamic structure of the TPHSL revealed by the CRA-Interim datasets agrees with that revealed by the ERA-Interim datasets. The TPHSL is located in the positive vorticity zone which inclines northward along the TPHSL from the lower layer to the upper layer, but the intensity of vorticity of the CRA-Interim datasets is stronger. The TPHSL corresponds to the convergence zone with an ascending motion which extends to 300 hPa; however, it is more complete and continuous for the CRA-Interim datasets.

(4) The thermal structure of the TPHSL revealed by the two datasets is basically consistent, and the CRA-Interim datasets show better applicability in the water vapor thermal structure. The contours of θ_{se} near the TPHSL tend to be intensive. In the vertical direction, the TPHSL analyzed with the CRA-Interim datasets is located in the transition belt between the warm-moist air and cold-dry air, while that analyzed with the ERA-Interim datasets penetrates into the dry and cold air on the north side with the obvious frontal zone near it.

(5) The characteristics of the dynamic and water vapor thermal structure in the east and west part of the TPHSL analyzed with the two datasets show good similarity. However, for the dynamic structure, there are more similar in the east part of TPHSL below 300 hPa compared with the west part of the TPHSL. And compared with the dynamic fields, the water vapor thermal fields in the east and west part of the TPHSL analyzed with the two datasets are more consistent.

(6) The CRA-Interim datasets show excellent attributes in the analysis and study of this TPHSL's structural characteristics; thus it should be reliable. In addition, the work in this paper is only based on one TPHSL case. Therefore, further analyses with more CRA-Interim datasets are needed. More importantly, it is necessary to investigate the comprehensive application of the two datasets in weather analysis and forecasting in the future.

REFERENCES

[1] BERRISFORD P, DEE D, POLI P, et al. The ERA-Interim Archive Verison 2.0 [M]. Shinfield Park, Reading: ECMWF, 2011: 1-27, https://www.ecmwf.int/node/8174.

[2] TIAN Y R, LI G P, LIU Y F. Comparison of the atmospheric heat source over the Tibetan Plateau computed by three reanalysis data sets [J]. Desert and Oasis Meteorology, 2017, 11(04): 1-8 (in Chinese).

[3] HE D Y, TIAN H, DENG W T. Applicability analysis of three reanalysis surface temperature data over the Tibetan Plateau [J]. Trans Atmos Sci, 2013, 36(04): 458-465 (in Chinese).

[4] HU M L, YOU Q L, LIN H B. Comparative analyses of geopotential height and wind field from multiple reanalysis

data over the Tibetan Plateau [J]. J Glaciology and Geocryology, 2015, 37(05): 1229-1244 (in Chinese).
[5] LIU C, LIU Y M, LIU B Q. Comparison of six sensible heat flux datasets over the Iranian-Tibetan Plateaus [J]. J Atmos Sci, 2015, 35(04): 398-404 (in Chinese).
[6] WANG M Y, YAO S, JIANG L P, et al. Collection and pre-processing of satellite remote sensing data in CRA-40 (CMA's global atmospheric reanalysis) [J]. Adv Meteor Sci Technol, 2018, 8(1): 158-163 (in Chinese).
[7] FLOHN H. Large-scale aspects of the "summer monsoon" in South and East Asia [J]. J Meteor Soc Japan, 1957, 75: 180-186, https://doi.org/10.2151/jmsj1923.35A.0_180.
[8] YIN M T. Synoptic-aerologic study of the onset of the summer monsoon over India and Burma [J]. J Atmos Sci, 1949, 6(6): 393-400, https://doi. org / 10.1175 / 1520-0469 (1949)006<0393: sasoto>2.0.co;2.
[9] TANAKA K, ISHIKAWA H, HAYASHI T, et al. Surface energy budget at Amdo on the Tibetan Plateau using GAME/Tibet IOP98 data [J]. J Meteor Soc Japan, 2001, 79 (1B): 505-517, https://doi.org/10.2151/jmsj.79.505.
[10] UEDA H, KAMAHORI H, YAMAZAKI N. Seasonal contrasting features of heat and moisture budgets between the eastern and western Tibetan Plateau during the GAME IOP [J]. J Climate, 2003, 16(14): 2309-2324, https://doi.org/10.1175/2757.1.
[11] YAO Xiu-ping, ZHANG Xia, MA Jia-li. Characteristics of the meridionally oriented shear lines over the Tibetan Plateau and its relationship with rainstorms in the boreal summer half-year [J]. J Trop Meteor, 2020, 26(1): 93-102, https://doi.org/10.16555/j.1006-8775.2020.009.
[12] ZHAO Fu-hu, LI Guo-ping, HUANG Chu-hui, et al. Modulation of Madden-Julian Oscillation on Tibetan Plateau vortex [J]. J Trop Meteor, 2016, 22(1): 30-41, https://doi.org/10.16555/j.1006-8775.2016.01.004.
[13] MURAKAMI T. The sudden change of upper westerlies near the Tibetan Plateau at the beginning of summer season [J]. J Meteor Soc Japan, 1958, 36(6): 239-247, https://doi.org/ 10.2151/jms j1923.36.6_239.
[14] LUO S W. Formation analysis of shear line over the eastern Plateau in winter [J]. Acta Meteor Sinica, 1963, 33 (3): 305-319 (in Chinese).
[15] XU G C. The climatologically synoptic characteristics of the shear line on the 500mb surface over the Qinghai-Xizang Plateau [J]. Plateau Meteor, 1984, 3(1): 38-43 (in Chinese).
[16] SHEN R, REITER E R, BRESCH J F. Numerical simulation of the development of vortices over the Qinghai-Xizang (Tibet) Plateau [J]. Meteor Atmos Phys, 1986, 35(1-2): 70-95, https: //doi. org / 10.1007 / bf01029526.
[17] GAO Yuan, YAO Xiu-ping. Impact of dynamic and thermal forcing on the intensity evolution of the vortices over the Tibetan Plateau in Boreal Summer [J]. J Trop Meteor, 2020, 26(2): 239-252, https://doi. org / 10.46267 / j.1006-8775.2020.022.
[18] ZHANG X, YAO X P, MA J L, et al. Climatology of transverse shear lines related to heavy rainfall over the Tibetan Plateau during Boreal Summer [J]. J Meteor Res, 2016, 30(6): 915-926, https://doi.org/10.1007/s13351-016-6952-7.
[19] YE D Z, LUO S W, ZHU B Z. The wind structure and heat balance in the lower troposphere over Tibetan Plateau and its surrounding [J]. Acta Meteor Sinica, 1957, 28(2): 108-121 (in Chinese).
[20] QIAO Q M, TAN H Q. The structure of 500mb shear line and large-scale circulation over Qingzang Plateau in summer [J]. Plateau Meteor, 1984, 3(3): 50-57 (in Chinese).
[21] LI G P. The Dynamic Meteorology Study of Tibetan Plateau [M]. Beijing: China Meteorological Press, 2002:1-251 (in Chinese).
[22] LI R, MIN Q L, WU X Q, et al. Retrieving latent heating vertical structure from cloud and precipitation profiles-Part II Deep convection and stratiform rain progresses [J]. J Quant Spectrosc Ra, 2013, 122: 47-63, https://doi. org / 10.1016/j.jqsrt.2012.11.029.
[23] YU S H, GAO W L, PENG J. Statistical analysis of shearline activity in QXP and its influence on rainfall in China in recent 13 years [J]. Meteor, 2013, 32(6): 1527-1537 (in Chinese).
[24] YAO X P, SUN J Y, KANG L, et al. Advances on research of shear convergence line over Qinghai-Xizang Plateau [J]. Plateau Meteor, 2014, 33(1): 294-300 (in Chinese).
[25] The Tibetan Plateau Science Research Group. Study on 500 hPa Low Vortex Shear Line of Tibet Plateau [M]. Beijing: Science Press, 1981: 100-122 (in Chinese).
[26] TAO S Y, LUO S W, ZHANG H C. The meteorological science experiment and observation system of the Qinghai-Tibet Plateau in May-August 1979 [J]. Meteor Mon, 1984, 10(7): 2-5 (in Chinese).
[27] TAO W K, SMITH E A, ADLER R F, et al. Retrieval of latent heating from TRMM measurements [J]. Bull Amer Meteor Soc, 2006, 87(11): 1555-1572, https://doi. org / 10.1175/ bams-87-11-1555.
[28] MIN Q L, LI R, WU X Q, et al. Retrieving latent heating vertical structure from cloud and precipitation profiles-Part I Warm rain processes [J]. J Quant Spectrosc Ra, 2013, 122: 31-46, https://doi. org / 10.1016 / j. jqsrt.2012.11.030.
[29] DEE D P, UPPALA S M, SIMMONS A J, et al. The ERA-Interim reanalysis: configuration and performance of the data assimilation system [J]. Quart J Roy Meteor Soc, 2011, 137(656): 553-597, https://doi.org/10.1002/qj.828.
[30] LIU Z M, LI G P. Objective identification of the Tibetan Plateau shear line and statistical analysis of its spatiotemporal evolution features [J]. Chin J Atmos Sci, 2019, 43(1): 13-26 (in Chinese).
[31] GUAN Q, YAO X P, LI Q P, et al. Study of a horizontal shear line over the Qinghai-Tibetan Plateau and the impact of diabatic heating on its evolution [J]. J Meteor Res, 2018, 32(4): 612-626, https://doi. org / 10.1007 / s13351-018-7186-7.
[32] MA J L, YAO X P. Statistical analysis of the shear lines and torrential rains over the Yangtze-Huaihe river region during June-July in 1981-2013 [J]. Acta Meteor Sinica, 2015, 73(5): 883-894 (in Chinese).

Citation: YAO Xiu-ping, ZHANG Shuo, BAO Xiao-hong, et al. Study on the structure of a horizontal shear line over the Tibetan Plateau based on CRA-Interim datasets and its comparison with ERA-Interim datasets [J]. J Trop Meteor, 2020, 26(4): 483-494, https://doi.org/10.46267/j.1006-8775.2020.042.